JOURNAL OF AIRCRAFT
Vol. 43, No. 4, July–August 2006

Development of Mach Scale Rotors with Tailored Composite Coupling for Vibration Reduction

Jinsong Bao,* V. T. Nagaraj,† and Inderjit Chopra‡
University of Maryland, College Park, Maryland 20742
and
Andreas P. F. Bernhard§
Sikorsky Aircraft Corporation, Stratford, Connecticut 06615

DOI: 10.2514/1.15484

This paper presents the design, structural and aeroelastic analyses, fabrication, and structural tests of Mach-scale articulated composite rotors with tailored flap-bending/torsion couplings for vibration reduction. The rotor design was nominally based on the UH-60 Black Hawk rotor. A new fabrication process was developed to manufacture Mach-scale composite tailored blade. Five sets of Mach-scale composite tailored rotors were successfully fabricated in-house, including a baseline rotor without coupling, two rotors with uniform spanwise flap-bending/torsion couplings, and two rotors with spanwise segmented flap-bending/torsion couplings. Bench-top and nonrotating dynamic tests were performed to verify the structural analysis of these composite tailored blades. The measured results correlated well with predictions. Comprehensive aeroelastic analysis (using University of Maryland Advanced Rotorcraft Code) of these Mach-scale composite tailored rotors indicated that blade elastic flap-bending/torsion couplings can significantly impact rotor vibration characteristics. It was shown that spanwise segmented flap-bending/torsion couplings can provide larger rotor vibration reduction than uniform spanwise couplings.

Introduction

THE introduction of advanced composite materials in the 1960s opened a new field of aircraft design, because of the higher specific strength and stiffness, better corrosion resistance, better damage tolerance, and superior fatigue characteristics compared with metals. Furthermore, the intrinsic directional nature of composite materials enables expansion of the design space to include elastic coupling and elastic tailoring. Composite materials are finding wide spread application in production helicopters. For example, the rotor blade spars of the Sikorsky S-92 and the UH-60M are made from composite materials. Composite tailoring technology has been successfully applied to the fixed-wing aircraft; for example, the composite bending/torsion coupled forward swept wing of the Grumman X-29 experimental plane [1]. However, to date, no production helicopter with composite rotors incorporates composite tailored elastic couplings.

During the past decades, a wealth of analytic research on composite rotors has indicated that composite tailored elastic couplings can beneficially influence aeromechanical stability and vibration characteristics of a rotor. Pioneering work by Hong and Chopra [2] studied the effects of elastic couplings on aeroelastic stability in hover. Panda and Chopra [3] extended the analysis to include dynamics of the composite rotor in forward flight. Smith and Chopra [4,5] also studied the potential of tailored composite couplings to improve aeromechanical stability and reduce vibratory blade loads of a hingeless rotor in forward flight, and integrated the composite structural analysis into the early version of UMARC (University of Maryland Advanced Rotorcraft Code) [6]. Their analyses showed that composite chordwise-bending/torsion coupling had a significant influence on blade stability [2,3,5] and resulted in a small increase in 4/rev vibratory hub loads [5]. On the other hand, flap-bending/torsion and extension/torsion couplings slightly reduced 4/rev vibratory forces and moments, but had a negligible influence on aeroelastic stability [5]. Yuan, Friedmann, and Venkatesan [7,8] also studied the aeroelastic response and stability of a composite hingeless blade. Their research showed that the flap-bending/torsion coupling associated with tip sweep could induce aeroelastic instability. Fulton and Hodges [9,10] investigated the aeroelastic stability of composite hingeless rotor in hover. The study covered both extension/torsion and bending/torsion coupled composite blades. In some cases, the bending/torsion coupling was shown to increase blade stability.

Nixon [11] studied the potential for improving the performance and aeroelastic stability of tilt rotors through the use of composite coupled blades. It was shown that passive blade twist control via elastic extension/torsion coupling of the rotor blade can significantly improve tilt rotor aerodynamic performance. Tracy and Chopra [12] developed an improved warping model to analyze a composite bearingless rotor. The negative chordwise-bending/torsion couplings of H-section composite flex beam were predicted to have a stabilizing effect on the regressive lag mode in hover and forward flight. It was shown that several vibratory hub loads were modestly influenced by the introduction of chordwise-bending /torsion couplings in the flex beam. Floros and Smith [13] shaped the aeroelastically induced rotor twist distribution using different spar layup configurations in order to reduce blade stall and alleviate vibratory loads for both hingeless and articulated rotors. Their investigations showed that the angle of attack on the retreating blade can be reduced by introducing coupled elastic twist, resulting in a significant reduction in blade stall. Their tailored composite couplings did not produce significant improvements in all of the vibratory hub loads simultaneously.

Ganguli and Chopra [14,15] presented an aeroelastic optimization study for a soft in-plane hingeless rotor blade consisting of a two-cell rectangular composite box-beam spar. The design variables were the fiber angles of the box-beam walls for five equally spaced spanwise blade elements. The objective function was defined as the sum of the scalar norms of six nondimensional 4/rev hub loads. It was shown

Presented as Paper 1787 at the 44th AIAA/ASME/ASCE/AHS Structures, Structural Dynamics, and Material Conference, Norfolk, VA, 7–10 April 2003; received 10 January 2005; revision received 17 October 2005; accepted for publication 26 November 2005.

*Assistant Research Scientist, Department of Aerospace Engineering, 3181 Glenn L. Martin Hall; jbao@umd.edu.

†Senior Research Scientist, Department of Aerospace Engineering, 3181 Glenn L. Martin Hall; vnagaraj@umd.edu.

‡Alfred Gessow Professor & Director, Alfred Gessow Rotorcraft Center, 3181 Glenn L. Martin Hall; chopra@eng.umd.edu. Fellow AIAA.

§Senior Dynamicist, 6900 Main Street, Stratford, Mail Stop S317A; abernhard@sikorsky.com.

that an optimized flap-bending/torsion coupled design could reduce 4/rev vibratory hub forces and moments by 5 to 28% at an advance ratio of 0.3, compared with the uncoupled design. In contrast, it was shown that chordwise-bending/torsion coupling had a negligible influence on reduction of vibratory hub loads. Yuan and Friedmann [16] also applied aeroc optimization techniques to composite hingeless rotors with two-cell composite blades. It was shown that selecting 4/rev vertical shear as the objective function could result in notable reduction in the hub vertical load component, however, other hub load components could increase. These aeroelastic optimization analyses of composite tailored rotor [14–16] indicate a promising passive approach to reduce the rotor vibration without weight penalty and at no additional power requirement.

Several experimental studies have been conducted to verify structural analysis of composite coupled beams. Chandra and Chopra [17,18] fabricated nontwisted composite beams with various cross sections, including rectangular solid sections, I sections, box sections, and two-cell airfoil sections. These beams displayed extension/torsion, or bending/torsion couplings. However, they were not "flight worthy." The bench-top static tests [17,18] and the rotating tests in a vacuum chamber [19,20] were carried out to validate the structural analysis of composite beams. Rand [21] also conducted vacuum chamber rotating tests of composite coupled beams and studied the structural dynamics characteristics of composite beams. Their composite beams (with lengths of 0.914 m [19,20] and 0.285 m [21], respectively) were rotated up to 1000 rpm. Nixon [22], Minguet and Dugundji [23,24], and Bauchau et al. [25] also conducted the bench-top tests of composite beams to validate their structural analyses.

To date, there have been very few experimental investigations of the effect of composite tailored couplings on rotor aeroelasticity and vibration characteristics. Especially, no Mach-scale composite tailored rotor has been designed, fabricated, and tested. Tracy and Chopra [26] built composite coupled flex beams, and tested a four-bladed, six-foot diameter, Froude scale soft in-plane hingeless rotor on a hover stand. The main blade itself was uncoupled. Two sets of flex beams were fabricated: rectangular cross-section flexures with flap-bending/torsion coupling, and H-section flexures with chordwise-bending/torsion coupling. Negative chordwise-bending/torsion coupling was shown to significantly increase the lag mode stability, while flap-bending/torsion coupling had only a small effect on the lag damping. The experimental damping data were satisfactorily compared with their UMARC predictions. Done [27] mentioned that Westland Helicopter conducted experimental research of composite coupled rotors. However, no information of this research is available in the open literature.

Despite the fact that potential benefits of composite tailored couplings for aeromechanical stability and vibration reduction have been demonstrated by numerous analyses, there is a notable lack of experimental verification (mostly because of the absence of high quality Mach-scale composite tailored rotors). Hence, the need for a high quality reliable test data of a dynamically scaled composite tailored rotor was emphasized for validation studies [28].

For a Mach-scale composite tailored blade, the relatively small model blade cross-section profile, the high operating speed, and the pretwist, present unique challenges in the design of tooling and structure of the blade. Also, simple and effective processes need to be developed to reduce the cost and time of composite blade fabrication. The purpose of the present research is the development and experimental evaluation of Mach-scale rotors with composite tailored couplings for rotor vibration reduction. This paper focuses on design, fabrication and structural tests of five sets of Mach-scale composite tailored rotors with different configurations of flap-bending/torsion coupling.

Table 1 Parameters of composite tailored rotor

Rotor diameter, m	1.8288
Number of blades	4
Solidity	0.0943
Lock number	5.93
Rotor speed, rpm	2300
Hover tip Mach number	0.65
Blade airfoil	SC1095
Hinge offset	5.9%
Blade chord, m	0.0677
Pretwist, deg	−12

Rotor Parameters and Blade Structure

Determination of Rotor Parameters

The design of the present Mach-scale composite tailored rotor models was nominally based on the UH-60 Black Hawk rotor. Two primary design constraints are imposed by the dimensions of wind tunnel test section and the available hub components. The Glenn L. Martin Wind Tunnel in the University of Maryland has a test section of 3.3528×2.3622 m. The model rotor diameter is typically restricted to 45–55% of the wind tunnel width to avoid interference effects [29]. This translates to a maximum rotor diameter of 1.5088 to 1.8440 m. The existing articulated hub is a four-bladed, fully articulated rotor system with coincident flap and lead-lag hinges offset 0.054 m. The smaller the rotor radius the larger the effective hinge offset. For reference, the UH-60 has a hinge offset of 4.7%, which would require a model rotor diameter of 2.2982 m. Limited by these constraints, the diameter of Mach-scale composite tailored rotor was selected to be 1.8288 m, resulting in a flap hinge offset of 5.9%. The higher hinge offset of the model rotor results in a higher fundamental flap frequency of 1.05/rev than that of the UH-60 rotor (1.04/rev). However, the impact of the first flap frequency on the 4/rev vibratory hub loads is not critical.

The UH-60 Black Hawk standard rotor blade has a radius of 8.1788 m, a nominal chord of 0.5273 m, a rectangular blade planform with a swept tip and nonlinear twist. The nominal operating speed is 258 rpm, resulting in a hover tip Mach number of 0.65. The main blade profile is a cambered SC1094R8 airfoil, whereas the outboard profile is an SC1095 airfoil. The design of Mach-scale model rotor blade is nominally based on the UH-60 standard blade. To simplify fabrication, the blade design features a rectangular planform without tip sweep, a linear twist of -12° and a single airfoil section (SC1095). The Mach-scale operating speed is 2300 rpm. It should be noted that the chord was increased to match the chord/radius ratio of Sikorsky's new "Wide Chord Blade" for the UH-60M. The main parameters of the present Mach-scale composite tailored rotor are presented in Table 1.

Design of Blade Structure

The asymmetric SC1095 airfoil, with a relatively thin maximum thickness of 9.5%, blade pretwist, and the high operating speed present unique challenges in the design of the structure and tooling for Mach-scale model rotor blades. In addition, the high operating speed significantly increased the requirements on the hydraulic drive system for the rotor test stand. The primary structural design objective is to maintain structural integrity (i.e., provide adequate safety margin) at the test condition of maximum rotor speed (2300 rpm), advance ratio ($\mu = 0.3$), and thrust level ($C_T/\sigma = 0.08$). As shown in Fig. 1, the structure of the present Mach-scale composite tailored rotor blades comprises a composite D-spar (IM7/8552 graphite/epoxy prepreg laid up on a foam core mandrel with embedded leading edge weights), an aft foam core, a composite weave skin (IM7/8552 graphite/epoxy) and a composite blade root insert. The composite spar is the primary structural element of the blade, which not only carries the blade loads, but also provides the desired elastic couplings. The aft foam core and the blade skin are used to maintain the blade airfoil profile. The leading edge weights are used to ensure correct chordwise mass balance for aeroelastic stability. Six leading edge weights (machined to the SC1095 profile) are used per each blade (with an interweight spanwise gap of 0.0356 m).

The blade root insert is the key interconnection between the blade root and the attachment arm of the articulated hub. The blade loads

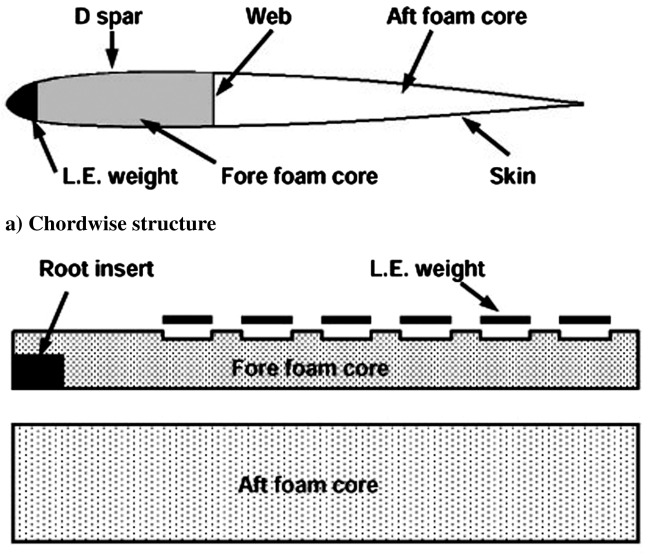

Fig. 1 Structure of Mach-scale composite tailored blade.

are transferred from the blade spar and skin to the root insert and finally to the hub. It is fabricated with a 0_{42} layup of IM7/8552 graphite/epoxy prepreg, with a length of 0.0559 m and a width of 0.0135 m. To examine the strength and the structural integrity of the root insert, a sample composite blade with this root insert was fabricated, and tension tested using an MTS material testing machine. The sample blade has the same composite layup as the Mach-scale composite blades. During the tensile testing, the first ply failure load of this composite blade insert was recorded. Defining first ply failure load as the load at first acoustic energy release, the measured first ply failure load was 1.1121×10^4 N. The root centrifugal force at blade grip (radial location 0.1905 m) is calculated to be 0.5384×10^4 N for the Mach-scale composite blades rotating at the nominal speed of 2300 rpm. It follows that this root insert design has an adequate safety margin, with a first ply failure safety factor of 2.1.

Layup Design of Composite D-Spar

Blade flap-bending/torsion couplings are introduced using a desired layup and orientation of composite plies in the composite D-spar. An important aspect of the D-spar design is to simultaneously achieve large elastic couplings, suitable frequency placement, and minimum stiffness difference between the baseline uncoupled blade and the coupled blades. Two sequential analysis tools were used to design the D-spar: the composite cross-section structural tool (required for computing blade section properties, including elastic coupling terms for a given unbalanced spar layup) and the subsequent comprehensive aeroelastic analysis to estimate the impact of elastic coupling on vibration. The design flow chart is shown in Fig. 2.

The structural analysis of the blade with the composite D-spar is based on the mixed force and displacement method presented by Jung, Nagaraj, and Chopra [30]. The cross-section structural equations for two-cell composite blade is given as

$$\begin{Bmatrix} Q_x \\ M_y \\ M_z \\ T_s \end{Bmatrix} = K \begin{Bmatrix} u' \\ \phi_y' \\ \phi_z' \\ \phi_x' \end{Bmatrix}$$

The blade axial, torsion, flap, and lag deformations are defined by u, ϕ_x, ϕ_y, and ϕ_z, respectively. The force Q_x, and the moments M_y, M_z, and T_s are associated with the axial, flap, lag, and torsion deformations. The coefficients k_{11}, k_{22}, k_{33}, k_{44}, and k_{24} of the cross-section stiffness matrix K are blade axial stiffness (EA), flap stiffness (EI_y), lag stiffness (EI_z), torsion stiffness (GJ), and flap-bending/

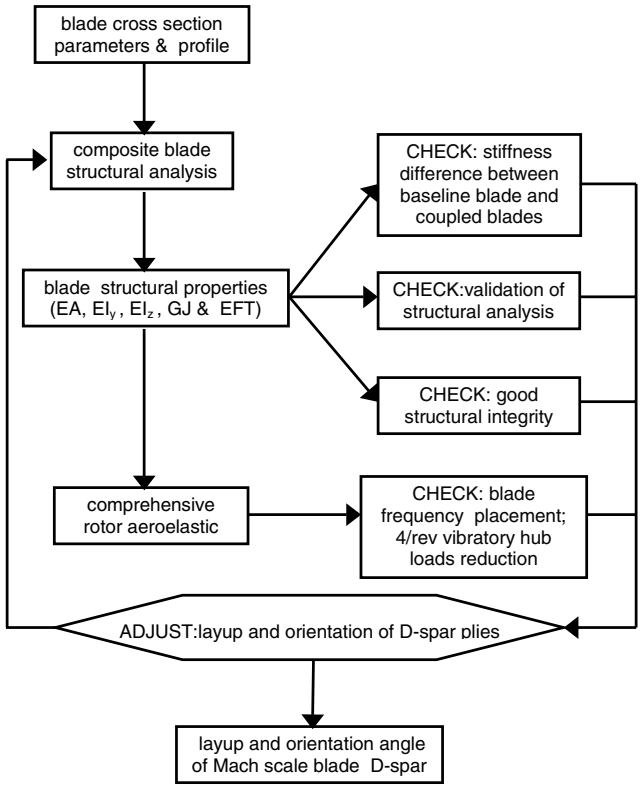

Fig. 2 Design flow chart of composite D-spar.

torsion coupling stiffness (EFT), respectively, and are given in the Appendix.

The aeroelastic analysis of composite tailored rotors is performed using a modified version of UMARC. This version can be used to perform the analysis of composite coupled rotors. The rotor-fuselage equations are formulated using Hamilton's principle and are discretized using finite elements in space and time. The effect of composite materials is introduced through the strain energy variation. The rotor blade is discretized in the spatial domain using 15 degrees of freedom beam finite element having axial, flap, lag, and torsion degrees of freedom. The aerodynamic analysis includes a free wake model. Rotor hub loads are calculated using the force summation method. The blade loads in the rotating system are then transformed to the fixed frame, and summed over the total number of blades to obtain the rotor hub loads. The vehicle trim and blade response solutions are calculated as one coupled solution. The blade

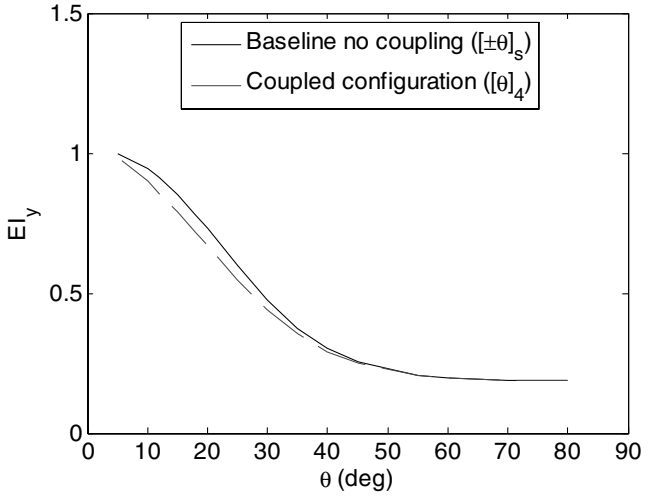

Fig. 3 Nondimensional flap stiffness (EI_y) of composite tailored blade versus fiber orientation angle of D-spar.

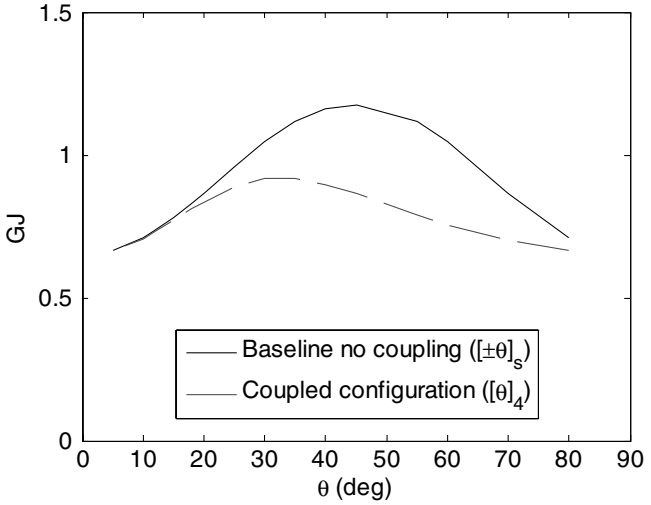

Fig. 4 Nondimensional torsion stiffness (GJ) of composite tailored blade versus fiber orientation angle of D-spar.

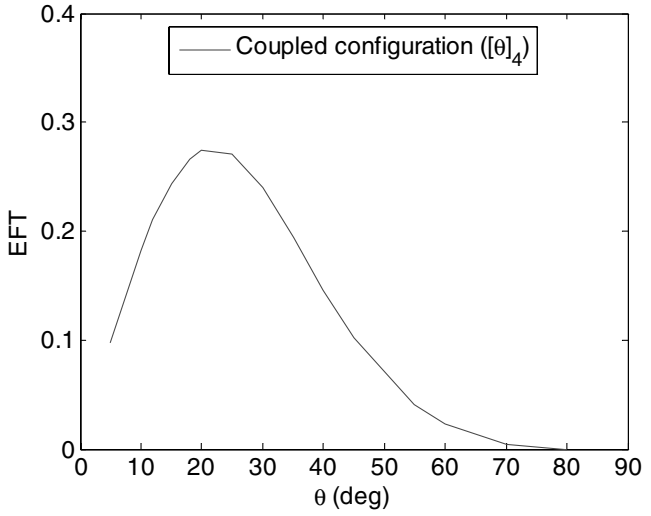

Fig. 5 Nondimensional flap-bending/torsion coupling stiffness (EFT) of composite tailored blade versus fiber orientation angle of D-spar.

response is computed using finite elements in time after the nonlinear equations in space are transformed into normal mode equations.

As shown in Fig. 2, there are three check points for the D-spar structural design: a) minimum stiffness difference between the baseline blade and the coupled blade, b) validation of the structural analysis (verified by the structural testing of sample blades), and c) good structural integrity (checked by the hover testing of sample blades). To study the structural behavior of these composite tailored D-spar blades, the variation of the structural stiffness with fiber orientation angles in the D-spar was analyzed. Blade cross-section stiffnesses of a baseline blade and a blade with flap-bending/torsion coupling are shown in Figs. 3–5. There stiffness values are normalized with respect to the baseline flap stiffness with a fiber orientation angle of 5°. The layups of these blades are listed in Table 2. Note that fiber orientation angle is defined as positive for the top wall of the D-spar when angled outboard from trailing to leading edge. The same fiber orientation is defined as negative for the bottom wall of the spar. In both blade configurations, the D-spar web is located at 33% chord. It is seen that the structural stiffnesses vary significantly with the spar orientation angle. As expected, the peak flap stiffness is achieved with 0° ply angle and decreases with increasing ply angle. The difference in flap stiffness between the coupled and baseline blade is relatively small, over the range of layup angles. In contrast, the torsion stiffness is low near ply angles of 0 and 90° and peaks in between. The difference in torsion stiffness between

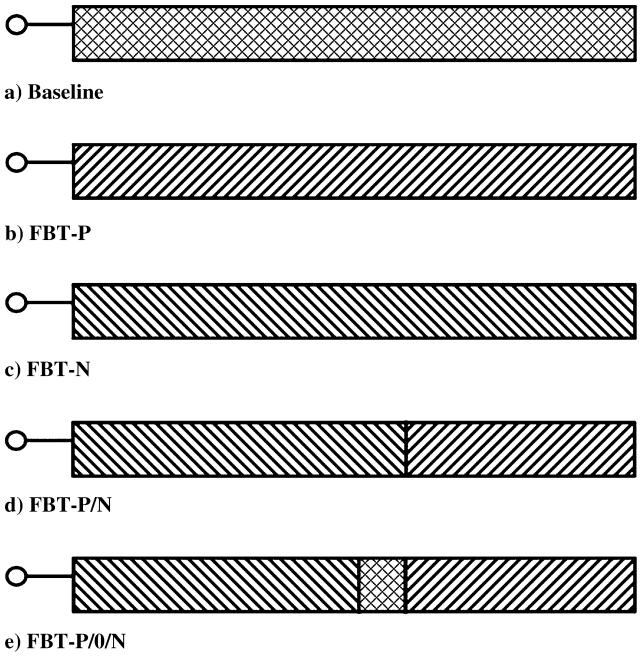

Fig. 6 Layup of different composite tailored blade configurations (top view of D-spar). FBT: flap-bending/torsion coupling; P: positive coupling; N: negative coupling; 0: no coupling; a) baseline uncoupled blade; b) uniform positive coupling; c) uniform negative coupling; d) spanwise segmented coupling (positive outboard and negative inboard; e) spanwise segmented coupling (positive outboard, uncoupled midspan, negative inboard).

the coupled and baseline blade is significant between ply angles of 25 and 75°. Furthermore, the ply angle for peak torsion stiffness is near 30° for the coupled blade, compared with 45° for the uncoupled blade. Figure 5 shows the effect of ply angle on the coupling stiffness. The largest flap-bending/torsion coupling is achieved with a spar fiber angle of around 20°. From these figures, it is evident that for a small scale rotor, there is limited design flexibility to simultaneously meet the primary design targets.

Following the structural analysis of the composite D-spar, comprehensive aeroelastic analysis (using UMARC) of the composite tailored rotor was performed to determine a) a suitable ply layup of the composite D-spar; and b) a suitable coupling distribution along the blade span. The objective of UMARC analysis was not only to check the frequencies placement, but also to seek the maximum reduction of 4/rev vibratory hub loads with suitable flap-bending/torsion coupling value and distribution.

After the iterative design process, five flap-bending/torsion coupling configurations of Mach-scale composite rotor were finalized; see Fig. 6. Positive flap-bending/torsion coupling of blade is defined as flap-up bending resulting in a nose-down twist. The first

Table 2 Layup of composite blade with two-cell D-spar

Skin	±45 weave
Baseline spar	Top: $[\pm\theta]_s$; bottom: $[-+\theta]_s$
Coupled spar	Top: $[\theta]_4$; bottom: $[-\theta]_4$
Web	$[\pm\theta]$

Table 3 Layup of Mach-scale composite tailored blades

Skin	±45 weave
Baseline spar	Top: $[\pm\theta_m]_s$; bottom: $[-+\theta_m]_s$
Positive flap-bending/torsion coupled spar	Top: $[\theta]_n$; bottom: $[-\theta]_n$
Negative flap-bending/torsion coupled spar	Top: $[-\theta]_n$; bottom: $[\theta]_n$
Web	$[\pm\theta]_p$
Web location	33% chord

Table 4 Normalized cross-section stiffness of Mach-scale composite tailored blade, with respect to baseline flap stiffness

Blade	Flap stiffness	Torsion stiffness	Coupling stiffness
Baseline	1.	0.838	0
Coupling	0.964	0.829	0.291

Table 5 Nondimensional natural frequencies of Mach-scale model rotor at rotor speed of 2300 rpm

	Baseline	FBT-P	FBT-N	FBT-P/N	FBT-P/0/N
Lag 1	0.327	0.327	0.327	0.327	0.327
Flap 1	1.052	1.052	1.052	1.052	1.052
Flap 2	2.673	2.640	2.640	2.642	2.652
Torsion 1	4.630	4.607	4.607	4.511	4.445
Flap 3	4.852	4.730	4.730	4.801	4.925
Lag 2	5.974	5.969	5.969	5.970	5.973

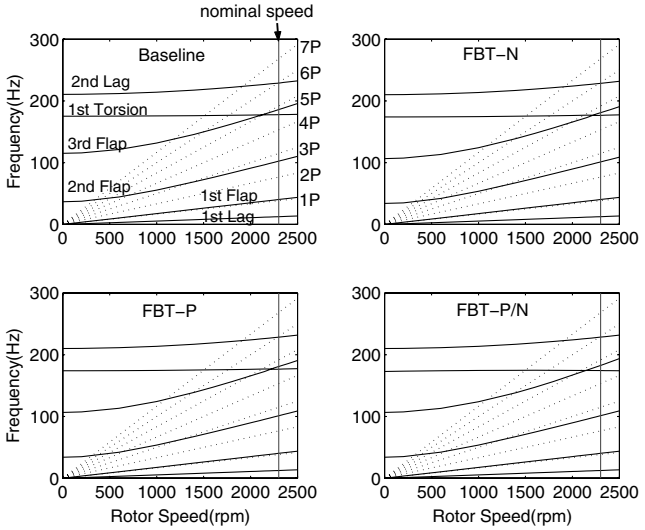

Fig. 7 Fan plots of Mach-scale composite tailored rotors.

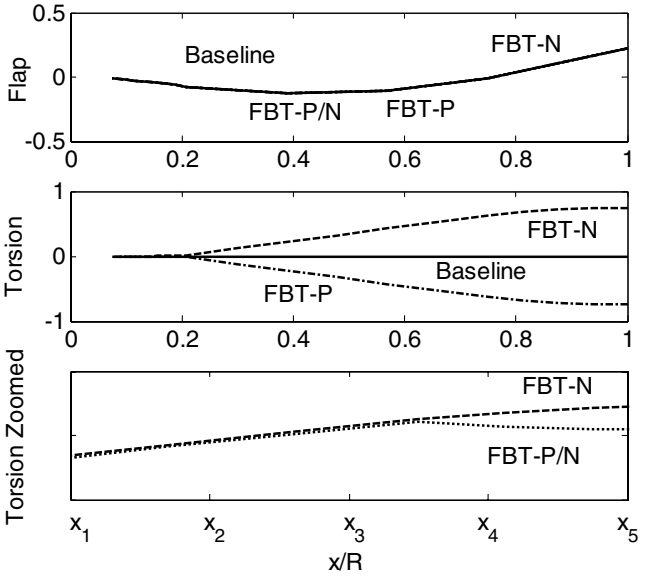

Fig. 8 The second flap mode shape of composite tailored blades.

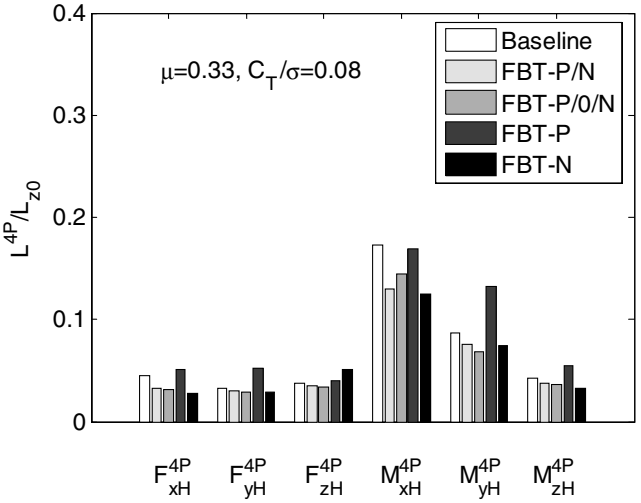

Fig. 9 Predicted 4/rev vibratory hub loads of Mach-scale composite tailored rotor models.

blade is a baseline blade with no coupling, the second and third blades exhibit spanwise uniform flap-bending/torsion coupling only (with the positive coupling designated FBT-P and the negative coupling designated FBT-N), and the last two blades feature spanwise segmented flap-bending/torsion couplings (designated FBT-P/N and FBT-P/0/N, respectively, and are also referred to as mixed-coupling rotors). Specifically, FBT-P/N incorporates a spanwise segmented coupling that is positive outboard and negative inboard; and FBT-P/0/N has a spanwise segmented coupling that is positive outboard, uncoupled in the midspan, and negative inboard. The layup of these Mach-scale composite tailored blades is tabulated in Table 3. The blade stiffness properties are listed in Table 4.

The fan plots of the Mach-scale composite rotors are shown in Fig. 7, and the natural frequencies at the nominal rotor operating speed of 2300 rpm are listed in Table 5. It is evident that the effect of the desired flap-bending/torsion coupling on the frequency placement is very small. The largest frequency difference between the mixed coupled (FBT-P/N) blade and the baseline blade is 2.5% in the torsion frequency. The relatively small frequency variation with couplings precludes frequency shifts dominating the impact of composite coupling on vibration characteristics. Figure 8 shows the mode shapes for the baseline and coupled rotor blades (specifically the first elastic mode). The torsion motion is significantly changed due to the introducing of flap-bending/torsion couplings, whereas the flap motion is same for all blade configurations. This change can significantly affect blade response and loads.

The predicted 4/rev vibratory hub loads for these Mach-scale rotors at an advance ratio of $\mu = 0.33$ with C_T/σ of 0.08 are presented in Fig. 9. The 4/rev vibratory hub forces, including drag force (F_{xH}^{4P}), side force (F_{yH}^{4P}), and normal force (F_{zH}^{4P}) are normalized with the baseline rotor steady normal force. Similarly, the 4/rev vibratory hub moments, including rolling moment (M_{xH}^{4P}), pitching moment (M_{yH}^{4P}) and yawing moment (M_{zH}^{4P}) are normalized with the

baseline rotor steady torque. The normalized 4/rev hub loads demonstrate notable differences between the baseline uncoupled rotor and the composite coupled rotors. This reflects the impact of the composite flap-bending/torsion couplings on the rotor vibratory loads. It is seen that composite tailored rotors with spanwise segmented couplings (FBT-P/N and FBT-P/0/N) have the overall best performance in terms of reducing all 4/rev hub loads. For example, for the spanwise triple-segmented coupling blade (FBT-P/0/N), the 4/rev normal force is reduced by 10%; and for the spanwise dual-segmented coupling blade (FBT-P/N), the 4/rev rolling moment is reduced by 25%. The analysis thus indicates that composite blade flap-bending/torsion couplings can be used to reduce vibratory hub loads with suitable tailoring and design optimization.

Fabrication of Composite Tailored Blade

A cost and time effective process is developed to fabricate the Mach-scale composite tailored blades, using a matched-die molding technique. A blade mold is designed and manufactured for the blade fabrication. There are six main steps to fabricate the present composite tailored blade. These are: a) forming the rigid foam core, b) assembly of leading edge weights and root insert, c) tailoring of composite prepreg, d) layup of the composite D-spar, e) assembly of complete blade and curing in the oven, and f) final blade finishing. The blade only needs to be cured once during the fabrication process.

The foam cores not only act as a layup mandrel for the composite D-spar, but also maintain the airfoil profile of the blade. For the present Mach-scale blades, the fore cell foam core is made from Rohacell IG-71, whereas the aft cell is made from Rohacell IG-31. The higher density IG-71 is selected for the leading edge cell, because it acts as a layup mandrel for the spar and it also provides improved support for the leading edge weights bonded inside the leading edge curvature of the spar. To form the blade foam core, a rectangular Rohacell blank is sanded to an approximate SC1095 airfoil shape and is then formed in the closed mold under temperature and pressure. To provide a space for the root insert, a small foam piece is cut from the root of the fore foam core. Six leading edge weight slots are also precisely milled into the leading edge of the fore cell foam core using a CNC (computer numerical control) machine.

In preparation for the composite layup of the D-spar, unidirectional IM7/8552 prepreg tape is tailored into the composite lamina with a desired fiber orientation angle. Pre-layup actions also include the fabrication of the root insert and the leading edge weights. The composite root insert is assembled from 42 plies of unidirectional IM7/8552 prepreg strip with a length of 0.0559 m and a width of 0.0135 m. The tungsten leading edge weights were machined (with airfoil profile) from a tungsten plate, using electrical discharge machining.

The next step is to build up the spar layup on the fore cell foam mandrel with suitably orientated plies of IM7/8552 graphite epoxy. Alternating upper and lower spar layers are interlaced around the leading edge for structural integrity. Finally, the spar is mated with the aft foam cell and wrapped with the IM7/8552 weave skin. The composite blade assembly is cocured in the closed mold in the oven. After curing, the epoxy bead at the blade leading edge is removed using fine files and sand paper in order to obtain an aerodynamically clean leading edge. Thereafter, the blade is trimmed to the desired length (0.7772 m) and chord (0.0677 m) by a small CNC machine. The final fabrication step for the composite blade is to drill the bolt hole pattern for the blade grips into the blade root insert.

Five sets of composite tailored rotor blades were fabricated, including the baseline blades and the coupled blades with different flap-bending/torsion couplings (FBT-P, FBT-N, FBT-P/N, and FBT-P/0/N, respectively). Figure 10 shows one of the fabricated Mach-scale composite tailored blade with linear pretwist. Six blades were fabricated for each of the baseline and uniform coupled rotors (FBT-N and FBT-P), and seven blades were fabricated for each of the two mixed-coupling rotors (FBT-P/N and FBT-P/0/N). The extra blades were fabricated to a) permit selection of closest match blades for 4-bladed rotor wind tunnel testing, b) provide spare blades in the event of unforeseen damage, and c) provide specimens for destructive characterization. The average mass of the 32 blades that were fabricated is 0.1769 kg, with a maximum mass difference of 1.2%.

Fig. 10 Pretwisted Mach-scale composite tailored blade.

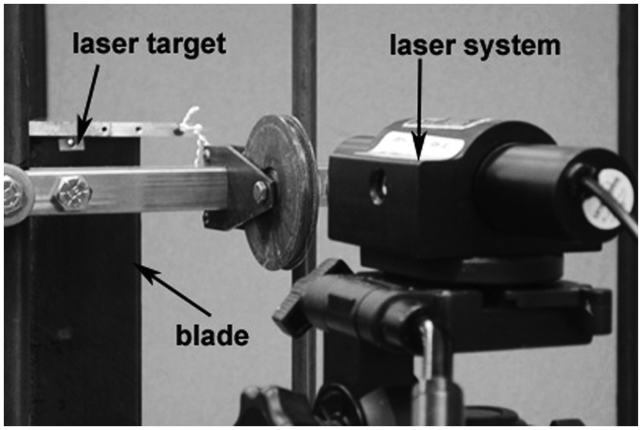

Fig. 11 Measurement setup for blade static deflection.

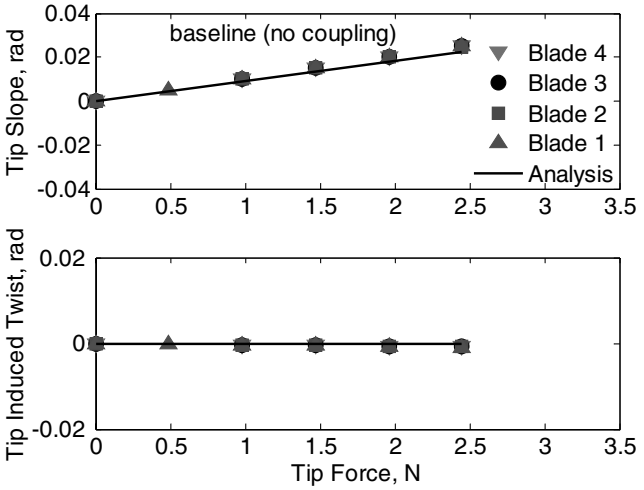

Fig. 12 Tip response of baseline composite blades under tip flapwise bending force.

Structural Tests

Bench-Top Testing

Before hover testing of the fabricated Mach-scale composite tailored rotors, a series of bench-top static tests, bench-top shaker tests, and nonrotating dynamic tests were performed to examine the blade structural properties.

The bench-top static test setup consists of a test stand and a laser optic system to measure blade deflections (see Fig. 11). The blade root is clamped in an airfoil shaped blade clamp that in turn is restrained between two steel plates of the test stand. Tip loads (transverse bending or torsion) are applied to the blade using dead weight loading, by means of a suitable arrangement of pulleys, loading lines, and an airfoil shaped clamp. A laser optical system and a mirror are used to measure blade tip bending slope and twist. A mirror is affixed to the blade tip and a laser beam bounced of the mirror onto a target screen. Blade tip bending slope and twist can be,

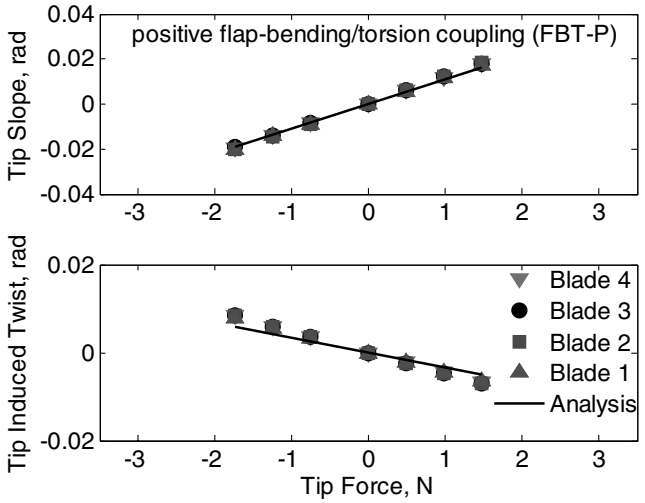

Fig. 13 Tip response of blades with positive flap-bending/torsion

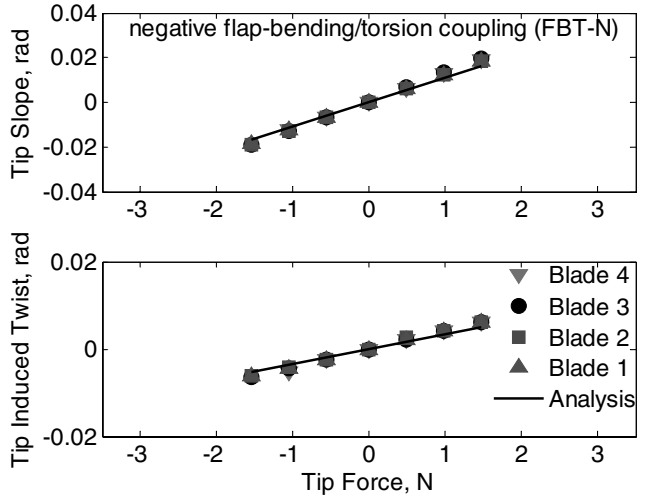

Fig. 14 Tip response of blades with negative flap-bending/torsion coupling (FBT-N) under tip flapwise bending force.

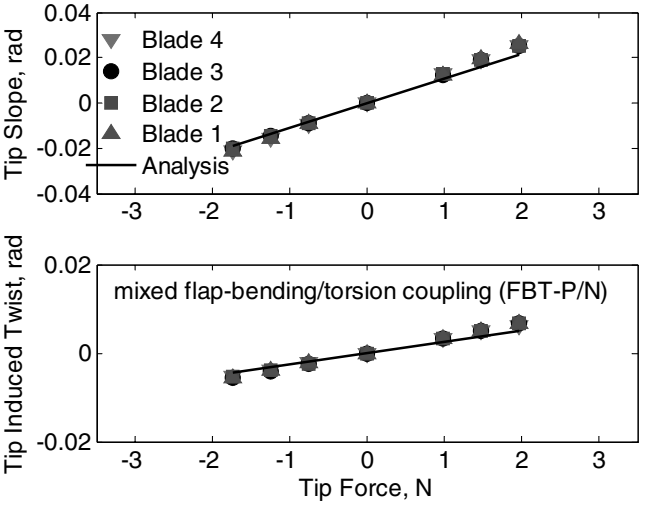

Fig. 15 Tip response of blades with mixed flap-bending/torsion coupling (FBT-P/N) under tip flapwise bending force.

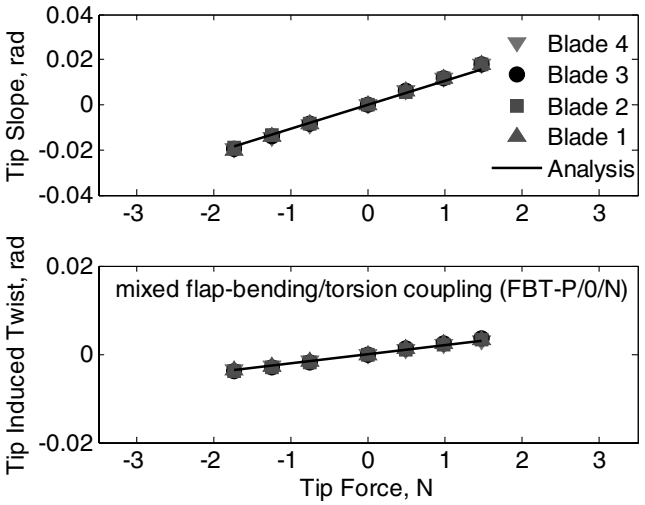

Fig. 16 Tip response of blades with mixed flap-bending/torsion coupling (FBT-P/0/N) under tip flapwise bending force.

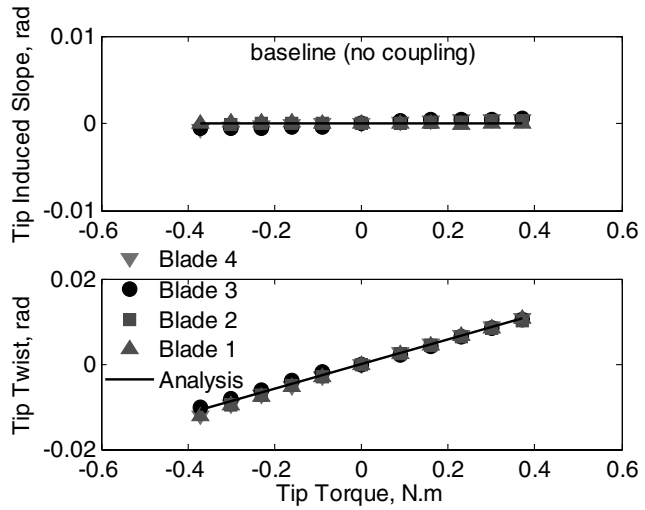

Fig. 17 Tip response of baseline blades under tip torque.

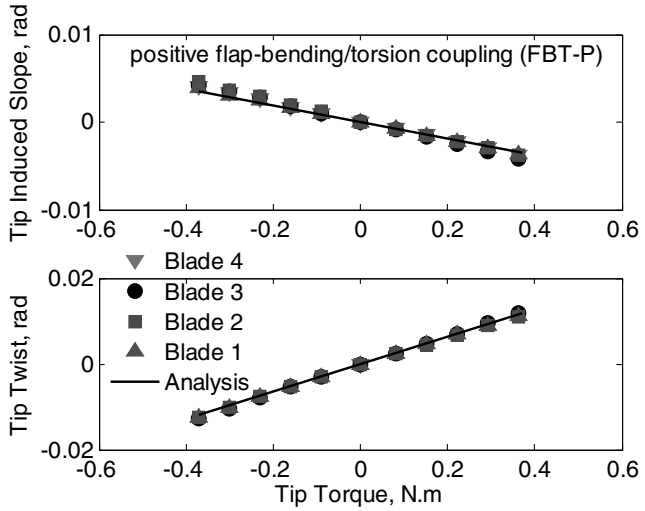

Fig. 18 Tip response of blades with positive flap-bending/torsion coupling (FBT-P) under tip torque.

respectively, computed from the vertical and horizontal displacement of the laser dot on the target screen.

Each of the fabricated blades was statically characterized using this test stand. Typically each blade was subjected to three transverse bending loads in both the flap-up and flap-down directions (except for the baseline uncoupled blades which were subjected to five transverse bending loads in the flap-up direction only); and five torque levels in both the nose-up and nose-down directions.

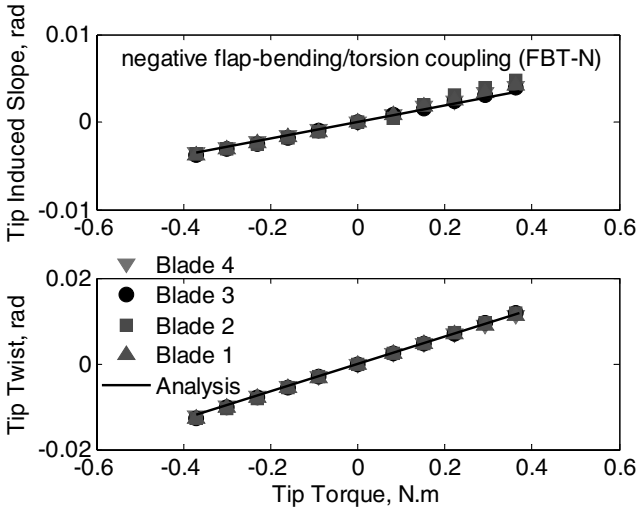

Fig. 19 Tip response of blades with negative flap-bending/torsion coupling (FBT-N) under tip torque.

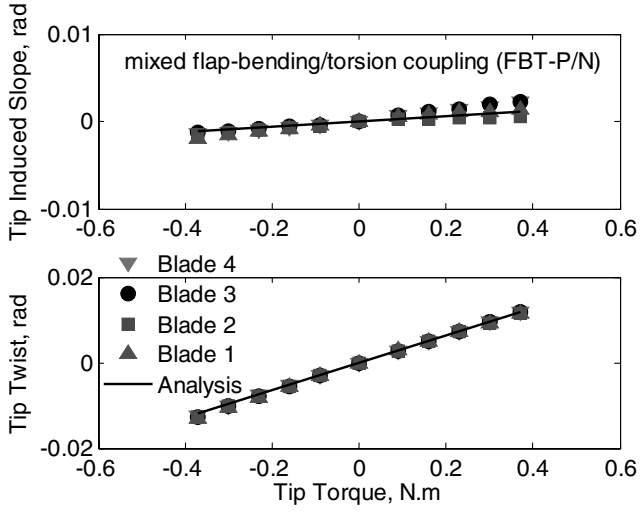

Fig. 20 Tip response of blades with mixed flap-bending/torsion coupling (FBT-P/N) under tip torque.

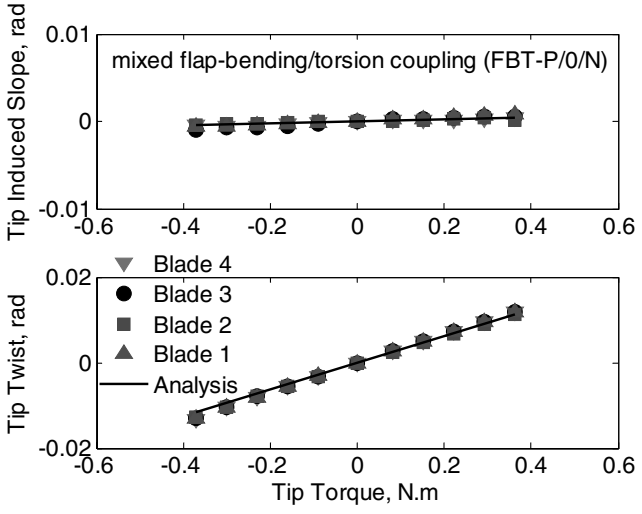

Fig. 21 Tip response of blades with mixed flap-bending/torsion coupling (FBT-P/0/N) under tip torque.

Figures 12–16 show the measured and predicted blade tip bending and twist under transverse tip bending for each of the five composite rotors; and Figs. 17–21 show the measured and predicted blade tip response under tip torque loading for each of the five composite rotors. Test data are shown for the four best matched blades for each rotor configuration. The blade tip deflection is analytically predicted using the force-displace relations of a cantilevered composite blade with flap-bending/torsion coupling:

$$\begin{Bmatrix} M \\ T \end{Bmatrix} = \begin{bmatrix} \mathrm{EI}_y & \mathrm{EFT} \\ \mathrm{EFT} & \mathrm{GJ} \end{bmatrix} \begin{Bmatrix} w'' \\ \phi_x' \end{Bmatrix}$$

where EI_y, GJ, and EFT are blade flap-bending stiffness, torsional stiffness, and flap-bending/torsion coupling stiffness, respectively. These stiffness properties are obtained from the blade cross-section structural analysis. w is flap-bending deflection and ϕ_x is blade-torsional deflection. M and T are the blade applied bending and torsion loads, respectively.

The bending slope (w_f') and bending-induced twist (ϕ_f) of a uniform cantilevered blade subject to a transverse tip bending force P are given by

$$w_f' = \frac{\mathrm{GJ}}{2(\mathrm{EI}_y\mathrm{GJ} - \mathrm{EFT}^2)} P(2lx - x^2),$$

$$\phi_f = \frac{\mathrm{EFT}}{2(\mathrm{EI}_y\mathrm{GJ} - \mathrm{EFT}^2)} P(2lx - x^2)$$

where l is the spanwise location of the applied force, and x is the spanwise location of the measurement point.

Similarly, the twist (ϕ_t) and torsion-induced bending slope (w_t') of a uniform cantilevered blade subjected to a tip torque are given by

$$w_t' = \frac{\mathrm{EFT}}{\mathrm{EFT}^2 - \mathrm{EI}_y\mathrm{GJ}} T_t x, \qquad \phi_t = \frac{\mathrm{EI}_y}{\mathrm{EI}_y\mathrm{GJ} - \mathrm{EFT}^2} T_t x$$

where T_t is the applied tip torque.

In general, the results presented in Figs. 12–21 show good correlation between analytic predictions and measurements; and good repeatability of the experimental data. Based on the measured data the four closest matched blades were selected from the six or seven blades fabricated for each rotor configuration.

Figures 12 and 17 demonstrate that the baseline blades neither twist under transverse tip bending, nor bend under tip torque loading. This confirms that the baseline indeed has no flap-bending/torsion coupling.

Figures 13 and 14, show that the coupled blades with respective uniform positive (FBT-P) and negative flap-bending/torsion coupling (FBT-N) have a similar coupling induced tip twist magnitude, but opposite sign (i.e., nose-up vs nose-down twist). Similarly, under tip torque loading the FBT-P and FBT-N blades exhibit similar magnitude but opposite sign induced blade tip bending; see Figs. 18 and 19. Essentially, the only different between the FBT-P coupled blade and the FBT-N coupled blade is the sign of the flap-bending/torsion coupling stiffnesses. For the FBT-P and FBT-N blades the induced twist is about 30% of the tip bending and the induced tip bending is approximate 35% of the tip twist, as expected from the ratio of coupling stiffness to direct bending stiffness and direct torsion stiffness.

Figures 15 and 16 show the tip bending-induced twist for each of the two different mixed flap-bending/torsion coupling blades (FBT-P/N and FBT-P/0/N). It is evident that the induced tip twist has the same sign as that of the negative coupled blade (see Fig. 14). The reason is that the blade tip response is dominated by the longer inboard spanwise extent of the negative coupling (see layup configurations of composite tailored blade in Fig. 6).

The structural analysis of the composite tailored blades was further validated by dynamic blade characterization, using bench-top shaker testing of a "sample" blade. This blade was fabricated using the same process as that described in the previous section. It has the same profile and dimensions as those of Mach-scale composite blades, but has a different layup of 33_4 spar, ± 45 skin, and ± 33 web (35%

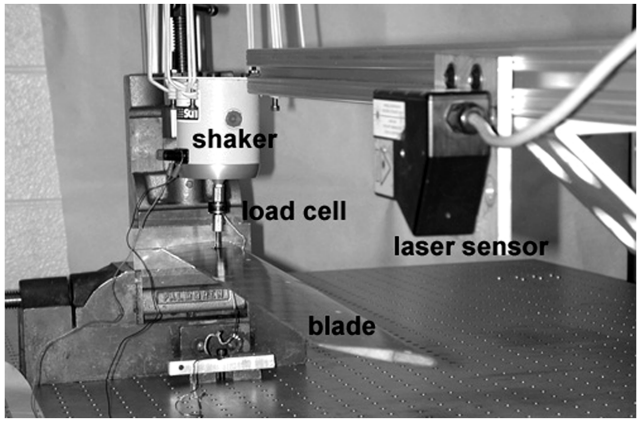

Fig. 22 Bench-top shaker test of a cantilevered composite tailored blade.

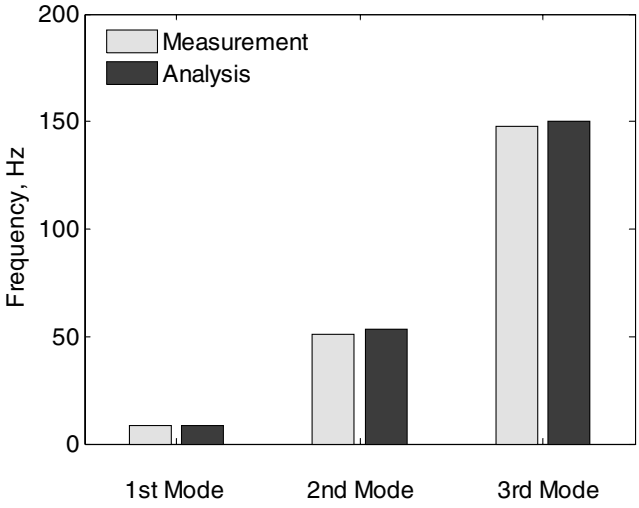

Fig. 23 Flapwise natural frequencies of a sample composite tailored blade: spar layup, 33_4; skin layup, ±45; web (35% chord), ±33.

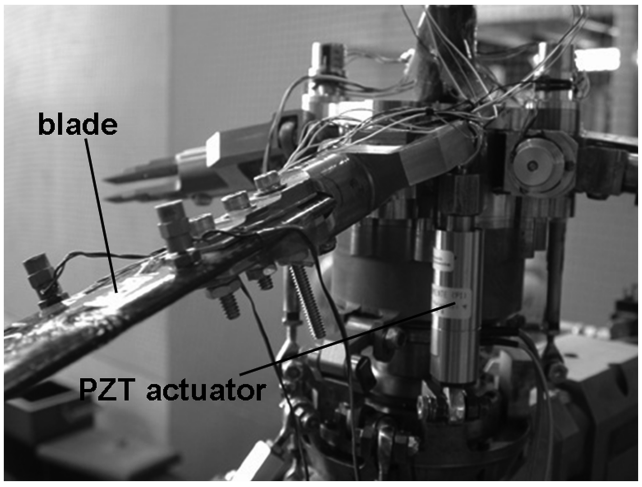

Fig. 24 Nonrotating dynamic test of composite tailored blade using a piezoelectric actuator.

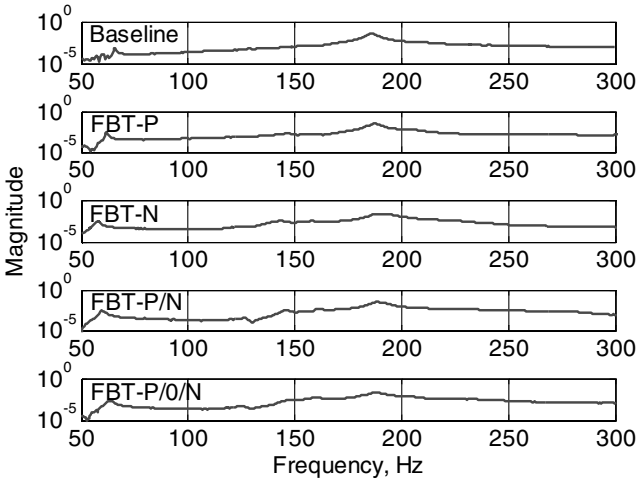

Fig. 25 Frequency response of nonrotating composite tailored blades.

chord). The dynamic test stand was set up on a vibration isolation table, as shown in Fig. 22. The composite blade was cantilevered using an airfoil shaped clamp that itself was clamped in a dual vice assembly. An electromagnetic shaker was suspended from a support frame with eight rubber cords to minimize spurious stiffness contributions. The shaker output force was applied to the blade through a load cell and a rigid rod. A laser sensor was used to measure the blade vibration response. Swept sine testing was performed with load cell feedback, to ensure constant force amplitude excitation. The predicted and measured first three natural frequencies are plotted in Fig. 23. Good correlation is demonstrated, with a maximum 2% difference between predicted and measured values.

Nonrotating Dynamic Testing

In addition to the bench-top tests, dynamic tests on the hover stand were performed to obtain the nonrotating fundamental torsion frequency of blades. The blade was mounted on the articulated hub and excited by a piezoelectric actuator installed as a temporary active pitch link, as shown in Fig. 24.

A SigLab system was used to perform swept sine tests from 50 to 300 Hz. The frequency response of the blade was measured by torsion strain gauges at 30% blade span. Five blades were tested, including the baseline blades and four coupled blades with different spanwise coupling configurations (see Fig. 6). The measured frequency responses of these blades are shown in Fig. 25. The dominant magnitude peaks of frequency response are 186, 186, 188, 188.5, and 187.5 Hz for the respective baseline, FBT-P, FBT-N, FBT-P/N, and FBT-P/0/N blades. That frequency is identified as the first nonrotating torsion frequency for these composite blades with hub connection. The predicted frequency is 177 Hz, corresponding to an underprediction of 5%. However, the difference of measured nonrotating torsion frequencies is within 1% between these composite tailored blades. It is evident that the effect of the flap-bending/torsion coupling on the frequency is very small.

Summary and Conclusions

Mach-scale composite tailored rotors have been developed for experimental evaluation of the effect of composite tailored flap-bending/torsion couplings on rotor vibratory hub loads. The design approach for these Mach-scale composite tailored rotors is presented. A new fabrication process is developed to manufacture Mach-scale composite tailored blade. Using this process, five sets of high quality composite tailored rotors were successfully fabricated with identical structural properties and good blade structural integrity, including a baseline rotor without coupling, two rotors with a uniform spanwise flap-bending/torsion coupling, and two rotors with spanwise segmented flap-bending/torsion coupling. A series of bench-top tests and nonrotating dynamic tests on the hover stand were performed to validate the structural analysis of these composite tailored blades. The test data show good correlation with the predictions. The aeroelastic analysis of these Mach-scale composite tailored rotors was carried out using a comprehensive rotor code (UMARC). It was found that spanwise segmented flap-bending/torsion couplings can provide larger overall rotor vibration reduction than uniform spanwise couplings.

It has been analytically demonstrated that composite blade flap-bending/torsion coupling can significantly impact rotor vibration characteristics, and with suitable design optimization can be manipulated to reduce vibratory hub loads.

Appendix

$$k_{11} = \int_s \left(A'_{11} - \frac{A'^2_{16}}{A'_{66}} \right) ds + \int_s \frac{1}{A'_{66}} C_u^2 ds,$$

$$k_{22} = \int_s \left(A'_{11} - \frac{A'^2_{16}}{A'_{66}} \right) z^2 ds + \int_s \frac{1}{A'_{66}} C_{\phi_y}^2 ds,$$

$$k_{24} = \int_s \frac{1}{A'_{66}} C_{\phi_y} C_{\phi_x} ds,$$

$$k_{33} = \int_s \left(A'_{11} - \frac{A'^2_{16}}{A'_{66}} \right) y^2 ds + \int_s \frac{1}{A'_{66}} C_{\phi_z}^2 ds, \qquad k_{44} = \int_s C_{\phi_x}^2 ds$$

where C_u, C_{ϕ_x}, C_{ϕ_y}, and C_{ϕ_z} are calculated for each cell of blade cross section.

$$C_u = \frac{\int_s \frac{A'_{16}}{A'_{66}} ds}{\int_s \frac{1}{A'_{66}} ds}, \qquad C_{\phi_x} = \frac{\int_s r ds}{\int_s \frac{1}{A'_{66}} ds},$$

$$C_{\phi_y} = \frac{\int_s \frac{A'_{16}}{A'_{66}} z ds}{\int_s \frac{1}{A'_{66}} ds}, \qquad C_{\phi_z} = \frac{\int_s \frac{A'_{16}}{A'_{66}} y ds}{\int_s \frac{1}{A'_{66}} ds}$$

The modified laminate stiffness A' is given by

$$A' = \begin{bmatrix} A_{11} - \frac{A_{12}^2}{A_{22}} & A_{16} - \frac{A_{12}A_{26}}{A_{22}} \\ A_{16} - \frac{A_{12}A_{26}}{A_{22}} & A_{66} - \frac{A_{26}^2}{A_{22}} \end{bmatrix}$$

where A is the classical lamination theory laminate stiffness matrix.

Acknowledgments

This work was supported with shared funding by the U.S. rotorcraft industry and government under the RITA/NASA Cooperative Agreement No. NCC2-9019, Advanced Rotorcraft Technology (01 January 2001). Technical Monitor was William Welsh from Sikorsky Aircraft Corporation.

References

[1] Ford, T., "New Shape in the Sky," *Aircraft Engineering*, Vol. 57, No. 9, 1985, pp. 2–5.

[2] Hong, C. H., and Chopra, I., "Aeroelastic Stability Analysis of a Composite Rotor Blade," *Journal of the American Helicopter Society*, Vol. 30, No. 2, 1985, pp. 57–67.

[3] Panda, B., and Chopra, I., "Dynamics of Composite Rotor Blades in Forward Flight," *Vertica*, Vol. 11, No. 1/2, 1987, pp. 187–209.

[4] Smith, E. C., and Chopra, I., "Formulation and Evaluation of an Analytical Model for Composite Box-Beams," *Journal of the American Helicopter Society*, Vol. 36, No. 3, 1991, pp. 23–35.

[5] Smith, E. C., and Chopra, I., "Aeroelastic Response, Loads and Stability of a Composite Rotor in Forward Flight," *AIAA Journal*, Vol. 31, No. 7, 1993, pp. 1265–1274.

[6] Bir, G., and Chopra, I., "University of Maryland Advanced Rotorcraft Code (UMARC) Theory Manual," Center for Rotorcraft Education and Research, University of Maryland, Technical Report UM-AERO 94-18, College Park, MD, July 1994.

[7] Yuan, K., Friedmann, P. P., and Venkatesan, C., "Aeroelastic Behavior of Composite Rotor Blades with Swept Tips," *Proceedings of the 48th American Helicopter Society Forum*, American Helicopter Society, Alexandria, VA, 1992, pp. 1039–1059.

[8] Yuan, K., Friedmann, P. P., and Venkatesan, C., "Aeroelastic Stability Response and Loads of Swept Tip Composite Rotor Blades in Forward Flight," *Proceedings of 35th AIAA/AHS/ASME/ASCE/ASC Structures, Structural Dynamics, and Materials Conference, Hilton Head, SC*, AIAA Paper No. 94-1309, 1994.

[9] Fulton, M. V., and Hodges, D. H., "Aeroelastic Stability of Composite Hingeless Rotor Blades in Hover-Part 1: Theory," *Mathematical and Computer Modelling*, Vol. 18, No. 3/4, 1993, pp. 1–18.

[10] Fulton, M. V., and Hodges, D. H., "Aeroelastic Stability of Composite Hingeless Rotor Blades in Hover-Part 2: Results," *Mathematical and Computer Modelling*, Vol. 18, No. 3/4, 1993, pp. 19–35.

[11] Nixon, M. W., "Aeroelastic Response and Stability of Tiltrotors with Elastically-Coupled Composite Rotor Blades," Ph.D. Dissertation, Department of Aerospace Engineering, University of Maryland, 1993.

[12] Tracy, A. L., and Chopra, I., "Aeroelastic Analysis of a Composite Bearingless Rotor in Forward Flight Using an Improved Warping Model," *Journal of the American Helicopter Society*, Vol. 40, No. 3, 1995, pp. 80–91.

[13] Floros, M. W., and Smith, E. C., "Elastically Tailored Rotor Blades for Stall Alleviation and Vibration Reduction," *Proceedings of the American Helicopter Society Aeromechanics Specialists' Meeting*, American Helicopter Society, Alexandria, VA, 2000.

[14] Ganguli, R., and Chopra, I., "Aeroelastic Optimization of a Helicopter Rotor to Reduce Vibration and Dynamic Stresses," *Journal of Aircraft*, Vol. 33, No. 4, 1996, pp. 808–815.

[15] Ganguli, R., and Chopra, I., "Aeroelastic Optimization of an Advanced Geometry Composite Helicopter Rotor," *Proceedings of 51st American Helicopter Society Forum*, American Helicopter Society, Alexandria, VA, 1995.

[16] Yuan, K. A., and Friedmann, P. P., "Structural Optimization for Vibratory Loads Reduction of Composite Helicopter Rotor Blades with Advanced Geometry Tips," *Journal of the American Helicopter Society*, Vol. 43, No. 3, 1998, pp. 246–256.

[17] Chandra, R., and Chopra, I., "Experimental and Theoretical Analysis of Composite I-Beams with Elastic Couplings," *AIAA Journal*, Vol. 29, No. 12, 1991, pp. 2197–2206.

[18] Chandra, R., and Chopra, I., "Structural Response of Composite Beams and Blades with Elastic Couplings," *Composites Engineering*, Vol. 2, Nos. 5–7, 1992, pp. 347–374.

[19] Chandra, R., and Chopra, I., "Experimental-Theoretical Investigation of the Vibration Characteristics of Rotating Composite Box Beams," *Journal of Aircraft*, Vol. 29, No. 4, 1992, pp. 657–664.

[20] Chandra, R., and Chopra, I., "Analytical-Experimental Investigation of Free-Vibration Characteristics of Rotating Composite I-Beams," *Journal of Aircraft*, Vol. 30, No. 6, 1993, pp. 927–934.

[21] Rand, O., "Experimental Investigation of Periodically Excited Rotating Composite Rotor Blades," *Journal of Aircraft*, Vol. 28, No. 12, 1991, pp. 876–883.

[22] Nixon, M. W., "Extension-Twist Coupling of Composite Circular Tubes with Application to Tilt Rotor Blade Design," *Proceedings of the 28th AIAA/ASME/ASCE/AHS Structures, Structural Dynamics, and Material Conference*, AIAA, Washington, DC, 1987, pp. 295–303; AIAA Paper No. 87-0772.

[23] Minguet, P., and Dugundji, J., "Experiments and Analysis for Composite Blades Under Large Deflections. Part 1: Static Behavior," *AIAA Journal*, Vol. 28, No. 9, 1990, pp. 1573–1580.

[24] Minguet, P., and Dugundji, J., "Experiments and Analysis for Composite Blades Under Large Deflections. Part 2: Dynamic Behavior," *AIAA Journal*, Vol. 28, No. 9, 1990, pp. 1581–1588.

[25] Bauchau, O. A., Coffenberry, B. S., and Rehfield, L. W., "Composite Box-Beam Analysis Theory and Experiments," *Journal of Reinforced Plastics and Composites*, Vol. 6, No. 1, 1987, pp. 25–35.

[26] Tracy, A. L., and Chopra, I., "Aeroelastic Stability Investigation of a Composite Hingeless Rotor in Hover," *Journal of Aircraft*, Vol. 35, No. 5, 1998, pp. 791–797.

[27] Done, G. T. S., "Rotorcraft Dynamics and Aeroelasticity Research in the U.K.," *Proceedings of the 6th International Workshop on Dynamics and Aeroelastic Stability Modeling of Rotorcraft Systems*, U.S. Army Research Office, University of California, Los Angeles, CA, 1995.

[28] Jung, S. N., Nagaraj, V. T., and Chopra, I., "Assessment of Composite Rotor Blade Modeling Techniques," *Journal of the American Helicopter Society*, Vol. 44, No. 3, 1999, pp. 188–205.

[29] Bi, N. P., "Contributions to the Experimental Investigation of Rotor/Body Aerodynamic Interactions," Ph.D. Dissertation, Department of Aerospace Engineering, University of Maryland, 1991.

[30] Jung, S. N., Nagaraj, V. T., and Chopra, I., "Refined Structural Model for Thin and Thick-Walled Composite Rotor Blades," *AIAA Journal*, Vol. 40, No. 1, 2002, pp. 105–116.